High Voltage

Research Article

IET Journals
The Institution of Engineering and Technology

Detailed electro-dynamic model of an ultra-fast disconnector including the failure mode

eISSN 2397-7264
Received on 20th December 2019
Revised 9th March 2020
Accepted on 26th March 2020
doi: 10.1049/hve.2019.0387
www.ietdl.org

Mario Zaja[1] ✉, *Ali Asghar Razi-Kazemi*[1], *Dragan Jovcic*[1]
[1]*School of Engineering, University of Aberdeen, AB24 3UE, Aberdeen, UK*
✉ *E-mail: m.zaja@abdn.ac.uk*

Abstract: Ultra-fast disconnector (UFD) is a key component of hybrid DC circuit breakers and it is also studied as the main switch in some DC grid topologies. A UFD model suitable for DC grid studies and considering both normal operation and failure mode is presented. The dynamic motion of contacts is analysed in detail and it is concluded that Thomson coil inductances including parasitic parameters play an important role and it is recommended to use finite element modelling. The arcing mode of UFD is repressed using a variable resistance in series with an ideal switch. The variable resistance is calculated analytically based on the instantaneous position of contacts and the circuit conditions. Two different arc models are recommended: for the air-insulated UFD and SF_6 UFD, and in each case, two operating regimes should be considered: high and low currents. The UFD model is verified for both normal operation and failure mode using measurements on a 5 kV laboratory UFD and the results show very good matching. The 320 kV SF6 UFD model is evaluated using limited reported results from manufacturers.

1 Introduction

High-voltage direct current (HVDC) transmission grids have been extensively studied as the means of integrating large renewable energy sources and strengthening network interconnection [1]. DC circuit breakers (DC CBs) play a critical role in DC grids, controlling the closing and opening of the circuits and isolating the faulted DC lines [2, 3]. The fast-rising, high-level short circuit currents in DC grids require high-speed protection devices, and the hybrid IGBT-based DC CBs have been developed for this application [4–6].

The ultra-fast disconnector (UFD) is a crucial component of hybrid DC CBs which determines their opening speed [4, 6]. The UFD should carry high load current with negligible loss and provide full voltage isolation in a very short time, i.e. 2 ms [4, 6]. The UFD can open only under very small current, i.e. 1 A [6], and this is ensured by the proper operation of other components in a hybrid DC CB [4]. The detailed study in [7] has demonstrated that the UFD current during opening will not be zero due to internal parasitics of the DC CB and the leakage through the commutation switch arrester.

The UFD can also be employed as a switching element on its own. In [8, 9], the UFD is used for fast isolation of faulted DC lines in meshed DC grids based on full-bridge modular-multilevel converters. The benefits are significant since the UFD is much lighter, faster and less expensive than a DC CB. UFDs are further used in many advanced DC CB topologies: four UFDs are employed to remove a semiconductor valve in a bidirectional DC CB in [10], a new method for controlling the voltage between UFD's contacts is shown to reduce fault current in the DC CB by 30% in [11], while in [12], a novel LC DC CB topology based on the fast commutation and controlled UFD voltage is proposed. In traditional bus-transfer switch applications a similar SF_6 disconnector is utilised [13–15].

Considering growing applications, an accurate electromechanical model of UFD is required for the system-level studies (transient stability, protection). An ideal switch model employed in [16] is only applicable if the UFD operates within its safe operating area (SOA) which assumes very low current and no overvoltage. An accurate UFD model is essential for new DC CB designs since the UFD is dynamically stressed very close to its dielectric breakdown voltage and the commutating current approaches limits.

Failure mode study of DC CB is provided in [17]. The scenarios for UFD failure are numerous and include spurious tripping, the failure of the current sensor in the auxiliary branch or the UFD driver failure [17]. A comprehensive UFD model is required to support such studies and estimate the stresses on the UFD and the rest of the components in the breaker.

For DC grid studies such as those in [7, 9], a detailed UFD model is required to verify that the voltage and current stresses on the UFDs during and after fault isolation do not violate the SOA and cause a restrike, with stability impact.

Some studies on UFD contact dynamics have been reported in [18] where the UFD is modelled as an electro-mechanical system with the driver, magnetically-coupled circuit and the dynamic mechanical system. Ritter *et al*. [13, 14] investigated SF_6 bus transfer switch under arcing but this is a very low voltage disconnector application.

This paper presents a comprehensive UFD model which links the dynamics of the electromechanical UFD model with the UFD failure mode model for accurately representing the UFD operation outside of the SOA. The aim is to develop a UFD model suitable for component and grid-level studies, which describes in adequate detail the UFD under arcing and the conditions for entering/exiting arcing mode for a practical 320 kV unit. The methodology adopted in the study is to:

(i) Develop an analytical model using MATLAB, COMSOL and PSCAD, for both normal and failure modes.
(ii) Verify the model on 5 kV UFD hardware prototype.
(iii) Extrapolate the model to represent a commercial 320 kV UFD, like those reported in [6, 19].

2 Electro-dynamic UFD model

2.1 Electrical circuit modelling: Thomson coil and driver

The structure of a prototype 5 kV UFD is shown in Fig. 1, which also represents the topology of commercial UFD although the number of breaking points will be higher [19]. TC (Thomson Coil) actuator provides the required energy for trip/close operation of the UFD and it is comprised of a primary stationary coil and a mobile conductive armature (disk plate) connected to the rod with contacts.

Fig. 2 illustrates the equivalent electrical circuit of the TC and the driver as implemented in our 5 kV prototype. When the

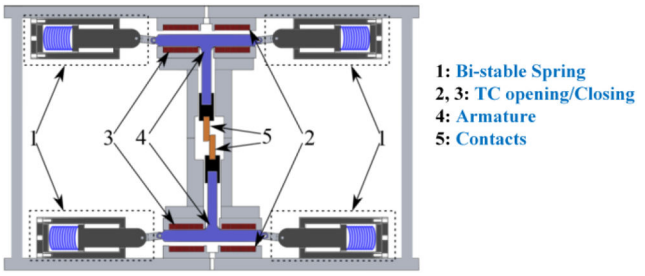

Fig. 1 *Main structure of the fabricated 5 kV UFD*

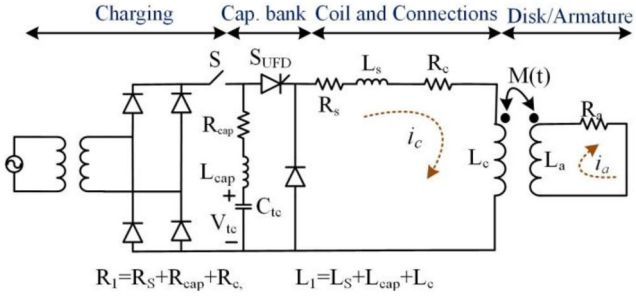

Fig. 2 *Equivalent electrical circuit of the TC and driver*

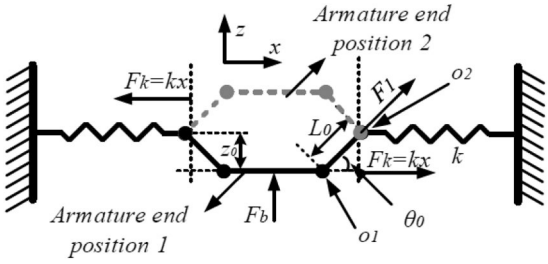

Fig. 3 *Bi-stable force diagram*

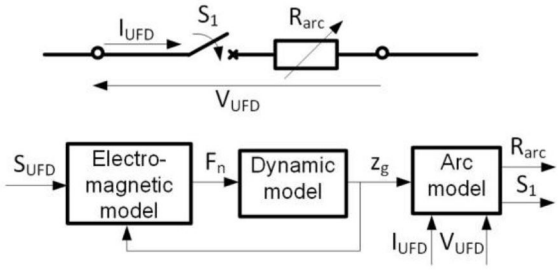

Fig. 4 *UFD model structure*

capacitor bank C_{tc} is charged to a voltage level V_{tc0}, the switch S is opened to isolate the driver from the power supply. The external signal from DC grid protection (or internal DC CB signal) S_{UFD} (trip/close command) will trigger the thyristor. The freewheeling diode provides current continuity. The current in the primary coil i_c, will induce current in armature i_a, through mutual inductance M, and the circuit model is expressed as:

$$\begin{aligned} &R_1 i_c + L_1 \frac{\mathrm{d}i_c}{\mathrm{d}t} - \frac{\mathrm{d}(Mi_a)}{\mathrm{d}t} = V_{tc} \\ &R_a i_a + L_a \frac{\mathrm{d}i_a}{\mathrm{d}t} - \frac{\mathrm{d}(Mi_c)}{\mathrm{d}t} = 0 \\ &R_1 = R_s + R_{Cap.} + R_c,\ L_1 = L_{Cap.} + L_s + L_c \end{aligned} \tag{1}$$

where R_C, R_s, R_c and R_a are the capacitor resistivity, stray resistivity of the connections, the primary coil resistivity, and armature resistivity, respectively, L_C, L_s, L_c, L_a and M are the capacitor inductance, stray inductance, coil inductance, armature inductance and mutual inductance, respectively.

The mutual inductance, which gives rise to the motion of the armature is dependent on the distance between coil and armature, and therefore it is time/position dependent. The variation of mutual inductance is expressed as a linear function:

$$M = M_0 - \frac{\mathrm{d}M}{\mathrm{d}z} z = M_0 - M'z \tag{2}$$

where M_0 (μH) is the initial value ($z = 0$), M' (μH/m) is the rate of change of the mutual inductance, and z (m) is the position of the armature. Therefore, (1) is simplified as:

$$R_1 i_1 + L_1 \frac{\mathrm{d}i_1}{\mathrm{d}t} - M\frac{\mathrm{d}i_a}{\mathrm{d}t} - i_a M' \frac{\mathrm{d}z}{\mathrm{d}t} = V_{tc} \tag{3}$$

$$R_a i_a + L_a \frac{\mathrm{d}i_a}{\mathrm{d}t} - M\frac{\mathrm{d}i_c}{\mathrm{d}t} - i_c M' \frac{\mathrm{d}z}{\mathrm{d}t} = 0\ . \tag{4}$$

2.2 Dynamic mechanical model

The force on armature (F_n) is expressed as follows:

$$F_n = F_e - F_f - F_b = m\frac{\mathrm{d}v}{\mathrm{d}t} = m\frac{\mathrm{d}^2 z}{\mathrm{d}t^2} \tag{5}$$

where F_e, F_f, F_b are the electromagnetic, friction and bistable forces respectively, v (m/s) is the operation speed of UFD, and m (kg) is the total mass of armature and the push/pull rod.

The electromagnetic energy in this system (w_e) is comprised of the stored energy in the coil, the armature and the mutual inductance, which is expressed as:

$$w_e = \frac{1}{2}L_c i_c^2 + \frac{1}{2}L_a i_a^2 - M i_a i_c \tag{6}$$

The electromagnetic force is obtained by differentiating (6):

$$F_e = -\frac{\mathrm{d}w_e}{\mathrm{d}z} = \frac{\mathrm{d}M}{\mathrm{d}z} i_a i_c \tag{7}$$

The bi-stable spring provides a force depending on the length, the position of the armature, and the stiffness of the springs as shown in Fig. 3 and can be modelled as [18]:

$$\begin{aligned} F_b &= 2k\frac{x_0 + |d| - \sqrt{L_0^2 - z_0^2}}{|d|}(z - z_0) \\ |d| &= \sqrt{L_0^2 - (z - z_0)^2} \end{aligned} \tag{8}$$

where x_0 is the pre-compression constant, z_0 and L_0 are the initial lengths as shown in Fig. 3; and k is the stiffness constant.

The friction force comprising of Columb and static friction has been modelled as a function of relative velocity [20]:

$$F_f = F_C + (F_s - F_C)\mathrm{e}^{-\left(\frac{v}{v_s}\right)^2} \tag{9}$$

where F_C and F_s are the Columb and the static frictions, respectively, and v_s is the Stribeck velocity (at peak value for Stribeck friction).

3 UFD model structure

Fig. 4 shows the proposed UFD model structure, consisting of an ideal switch S_1 (0-open, 1-closed) variable resistor R_{arc} and an analytical part. S_{UFD} (0/1) is the control signal received form the DC grid protection, F_n is the force on armature, z_g is the electrode gap analysed in Section 2, while R_{arc} is the arc model resistance studied in Section 4.

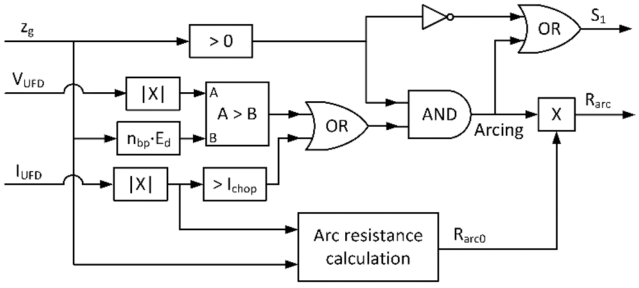

Fig. 5 *UFD arc model structure*

4 UFD failure mode model

4.1 Arc modelling in EMT software

This section aims to accurately represent UFD's behaviour outside of the SOA. The SOA is defined by the UFD's chopping current I_{chop} and UFD's maximum withstand voltage V_{max} so that $|I_{UFD}| \leq I_{chop}$ and $|V_{UFD}| \leq V_{max}$. Within the SOA, the UFD can enter open state and remain opened. On the other hand, opening the UFD under current larger than I_{chop} or stressing the contacts with voltage higher than V_{max} ignites an arc between the contacts. The arc creates a conducting channel in the gaseous insulating medium and the UFD remains a closed circuit with resistance R_{arc} despite its contacts being physically separated. The chopping current may depend on the contact geometry, contact distance and applied voltage, but this variation is small, and it is assumed that I_{chop} is constant. This value is typically small [21], e.g. $I_{chop} = 1$ A in SF_6 [6], while in air UFD $I_{chop} = 0.5$ A. Further analysis has demonstrated that the impact of chopping current is small since the load current is much larger (i.e. 2 kA). Since the UFD will not arc in normal operation, thermal phenomena are neglected in evaluating V_{max}. This means that V_{max} is solely dependent on the dielectric conditions and is represented as:

$$V_{max} = z_g E_d n_{bp} \tag{10}$$

$$z_g = \begin{cases} 2z - z_{ovl} z \geq \dfrac{z_{ovl}}{2} \\ 0 z < \dfrac{z_{ovl}}{2} \end{cases} \tag{11}$$

where z_{ovl} is the overlap of the contacts in the closed state, z_g is the gap distance, E_d is the dielectric strength of the insulating medium and n_{bp} is the number of breaking points.

The implementation of the electric arc in UFD model is shown in Fig. 5. S_1 is open if the UFD's contacts are separated $(z_g > 0)$ and there is no arcing, otherwise it is closed. The arc is active (Arcing = 1) if the contacts are separated and $|I_{UFD}| > I_{chop}$ or $|V_{UFD}| > V_{max}$.

The theoretical arc resistance R_{arc0} is continuously determined from the current magnitude and gap distance. The actual arc resistance is obtained by multiplying R_{arc0} with the Arcing signal. By setting Arcing to 1, resistor R_{arc} obtains a non-zero value which changes according to the grid conditions.

4.2 Arc resistance calculation in air

The calculations for R_{arc0} depend on the type of the insulating medium. For an air-insulated UFD (5 kV lab UFD), R_{arc0} is determined based on Paukert's arc model, using compilation of arc voltage measurements reported in [22]. Paukert's arc voltage compilation is one of the most comprehensive ones to date [23] and contains formulae for estimating the arc voltage for electrode distances up to 200 mm and currents up to 100 kA. It is also the only analytical arc model which estimates the arc voltage at low currents. In its basic form, Paukert's arc model is written as

$$V_{arc} = A\, I_{arc}^{B} \tag{12}$$

where I_{arc} is the arc current while A and B are empirically determined constants for a particular air gap distance and current range. Separate Paukert's coefficients at high and low currents are needed because the arc voltage increases with current in the high current range but decreases with the current in the low current range (negative resistance) [23]. The transition current at which this occurs in the Paukert's model is assumed as $I_t = 100$ A [22].

In its original form, Paukert's arc model is not suitable for this application since both the gap distance and current magnitude change dynamically with the operating conditions the UFD is subject to. It is, therefore, necessary for A and B to change as well. To ensure a smooth transition between various Paukert's coefficients, an interpolated Paukert's model is proposed.

The Paukert's coefficients A_1, B_1, A_2 and B_2, defined at air gap distances of z_{g1} and z_{g2}, respectively and belonging to the same current range, are used to determine the interpolated Paukert's coefficients are obtained as follows:

$$A_{12} = A_1 + \frac{A_2 - A_1}{z_{g2} - z_{g1}}\left(z_g - z_{g1}\right) \tag{13}$$

$$B_{12} = B_1 + \frac{B_2 - B_1}{z_{g2} - z_{g1}}\left(z_g - z_{g1}\right) \tag{14}$$

This interpolation makes A_{12} and B_{12} continuous smooth functions of z_g so that (12) covers a wide range of UFD air gap distances. The coefficients A_1, B_1, A_2 and B_2 are defined separately for currents above and below the transition current I_t. To combine two operating ranges into one smooth function, transition function $O(I_{arc})$ is defined as

$$O(I_{arc}) = \exp\left[-\left(\frac{I_{arc}}{I_t}\right)^2\right] \tag{15}$$

The finalised interpolated Paukert's model is given as

$$V_{arc} = [1 - O(I_{arc})]\, A_H I_{arc}^{B_H} + O(I_{arc})\, A_L I_{arc}^{B_L} \tag{16}$$

where A_H, B_H, for high current ($I_{arc} > I_t$) and A_L, B_L for low current ($I_{arc} < I_t$) are interpolated coefficients A_{12} and B_{12}. When the current is low, $O(I_{arc}) \simeq 1$ so $V_{arc} \simeq A_L I_{arc}^{B_L}$. Conversely, when current is high, $O(I_{arc}) \simeq 0$ so $V_{arc} \simeq A_H I_{arc}^{B_H}$. The pre-calculated arc resistance is obtained by dividing (16) with I_{arc}:

$$R_{arc0} = [1 - O(I_{arc})]\, A_H I_{arc}^{B_H - 1} + O(I_{arc})\, A_L I_{arc}^{B_L - 1} \tag{17}$$

Transforming the arc model from the voltage (16) to the resistance form (17) is advantageous because the resistance, unlike voltage, is independent of the current direction. This simplifies model, since (16) is not real if $I_{arc} < 0$ whereas (17) is evaluated using only the current magnitude.

4.3 Arc resistance calculation in SF_6

For high-voltage applications, the UFD is isolated using sulphur-hexafluoride (SF_6) rather than air [6]. Owing to its high dielectric strength, SF_6-insulated switchgear requires the smaller distance between contacts and has shorter operating time [24]. Despite its widespread use in the electric power industry, the knowledge about SF_6 arc modelling is limited, contrary to the arcs in the air where comprehensive experimental data is publicly available [22, 23].

A study on SF_6 arcs in DC disconnectors (in the function of a load transfer switch) concluded that the arc resistance at a fixed gap width is generally independent of the current magnitude [13–15]. The same conclusion has also been reached in earlier studies on SF_6 arcs [25]. It is assumed that the behaviour of arcs in conventional SF_6 disconnectors is similar to the behaviour of arcs in UFDs, and the arc model from [13–15] is adopted.

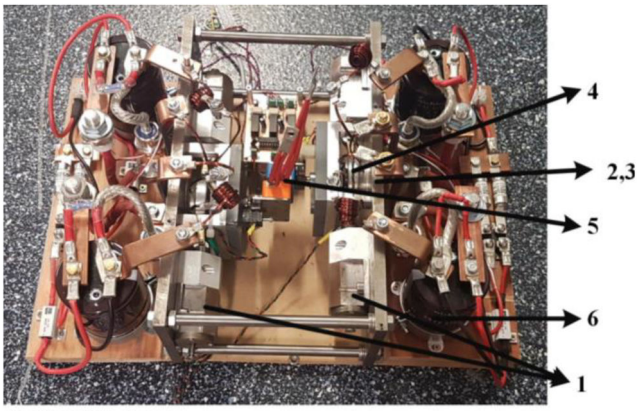

1: Bi-stable Spring
2, 3: TC opening/Closing
4: Armature
5: Contacts
6: TC Capacitor

Fig. 6 *Photograph of the laboratory 5 kV UFD*

Table 1 TC and driver design parameters for 5 and 320 kV UFD

Parameters	5 kV	320 kV
capacitor bank (C_{tc})	2.7 mF	11 mF
voltage (V_{tc})	300 V	900 V
R_C	15 mΩ	20 mΩ
disk radiuses (R_d)	25 mm	65 mm
disk thickness (T_d)	10 mm	30 mm
disk material	aluminum	Aluminum
thickness of holder (H_t)	4.5 mm	6 mm
height of holder (H_h)	7 mm	10 mm
holder martial	carbon steel	Carbon Steel
number of turns	9	20
coil width (C_w)	1.4 mm	2 mm
coil height (C_h)	2.75 mm	4 mm
inner radiuses of coil (R_i)	6.5 mm	27.5 mm
outer radius of coil (R_o)	21 mm	47.5 mm

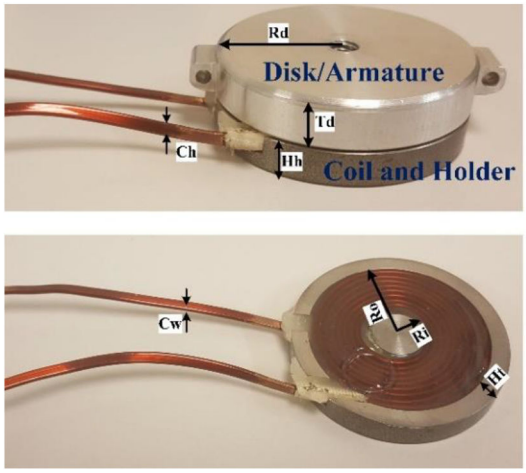

Fig. 7 *Laboratory TC (coil, holder and armature)*

Considering the data presented in [14, 15], it is evident that SF_6 arc voltage V_{arc} greatly depends on the gap distance z_g, and an analytical expression is derived as:

$$V_{arc} = 14.3 + 12.33 \cdot z_g^{0.64} \quad (V) \tag{18}$$

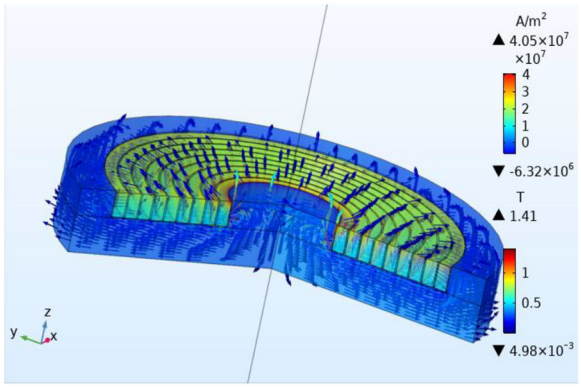

Fig. 8 *Current density and magnetic flux of the simulated TC- 5 kV UFD*

where z_g (mm) is gap distance. By dividing (18) with the arc current I_{arc}, the expression for SF_6 arc resistance is obtained as

$$R_{arc0} = \left(14.3 + 12.33 \cdot z_g^{0.64}\right) \cdot I_{arc}^{-1} \tag{19}$$

5 UFD model verification in normal operation

The UFD model is implemented in PSCAD, considering two test systems: 5 kV laboratory hardware and 320 kV commercial UFD.

5.1 5 kV hardware UFD demonstrator

Fig. 6 shows a photograph of the 5 kV UFD prototype while Table 1 presents the parameter values for TC and driver. This UFD is an upgrade on the UFD prototypes employed in experimental setups in [10–12] The TC and armature used in this UFD is shown in Fig. 7. Two nine-turn TCs are driven from 2700 μF capacitors at a voltage around 300 V to provide double (reciprocal) contact motion for opening/closing operation. The reciprocal motion results in an improvement in the contact separation speed. The mass of each moving assembly (armature, rod and contacts) is about 175 gr. The contacts maximum distance is about 3.5 mm. Our study not only indicates mutual inductance but also stray inductances and stray parameters which, as shown in (1)–(5), play a significant role in the model. Therefore, COMSOL Multiphysics software has been utilised to numerically evaluate the parameters for electromagnetic interactions.

Fig. 8 shows the current density and the magnetic flux in the holder and coil obtained by COMSOL for 5 kV UFD. As can be seen, the flux is denser in the centre and vertically distributed along the surface which is consistent with results in [18]. The self-inductance and the resistance of the coil (L_c, R_c) are measured on hardware (an RLC meter LCR-8101G) to confirm COMSOL results. However, it is not feasible to measure inductance and resistance of the disk-shaped armature and discriminate between the self and mutual inductances. These results have been compared with the analytical formula for a single-layer spiral coil as presented in [26]:

$$L_c = \frac{a^2 n^2}{8a + 11c}(\mu\text{H}) \qquad a = 0.5*(R_o + R_i), c = (R_o - R_i) \tag{20}$$

where n, a and c are the turn number of the coil, the average radius and the thickness of the coil, respectively.

Table 2 compares the result of analytical approach, measurement and COMSOL design for 5 kV UFD. As expected, when the holder is included, the inductance increases owing to the holder magnetic material. Also, when the armature is added, the total inductance of the coil is decreased because of the negative impact of the mutual inductance. Since the COMSOL FEM model is verified, the self and mutual inductances are calculated for a range of gap distances as presented in Fig. 9. It is seen that as the distance of the armature increases, the mutual inductance is decreasing (from ($M_0 = 0.047$ μH) at a specific rate of $M' = 0.0044$

Table 2 Verification of TC inductances for 5 kV UFD

Cases	Calculation approach	L, μH
spiral coil without holder	Analytical approach	2.08
—	COMSOL	1.95
coil and holder	Measurements	3.6
—	COMSOL	3.8
coil, holder and armature (z = 0 mm)	Measurements	1.41
—	COMSOL	1.42

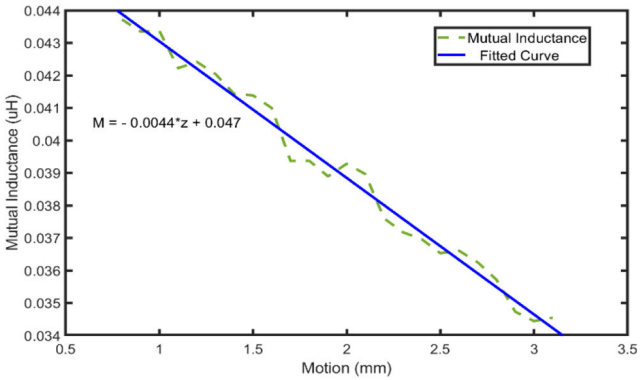

Fig. 9 *Variation of mutual inductances against motion for 5 kV UFD*

Table 3 Electrical Parameters for 5 and 320 kV UFD

TC Parameters	5 kV	320 kV
L_c, μH	3.6	71
L_a, nH	1	4
R_c, mΩ	7	30
R_a, mΩ	0.003	0.004
M_0, μH	0.047	0.42
M', μH/mm	0.0044	0.0084

Table 4 Design parameters for 5 and 320 kV UFD

Rated voltage	320 kV	5 kV
dielectric strength	9 kV/mm.bar	3 kV/mm.bar
total gap distance	60 mm	3.5 mm
maximum travel distance	8.5 mm (5 breaking points)	3 mm
moving mass	3.5 kg	175 gr
friction parameters	F_C = 30 N, F_s = 80 N, v_s = 5 m/s	F_C = 15 N, F_s = 35 N, v_s = 4 m/s
bi-stable system	Spring const. = 300 N/mm, overlap = 4.25 mm	Spring const. = 30 N/mm, overlap = 1.5 mm

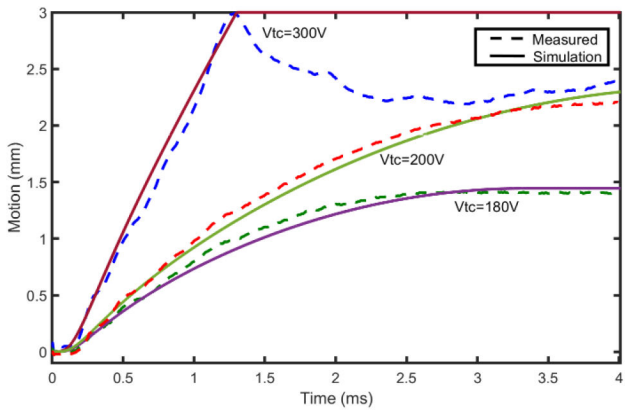

Fig. 10 *Measured motion curves and the simulated curves in PSCAD*

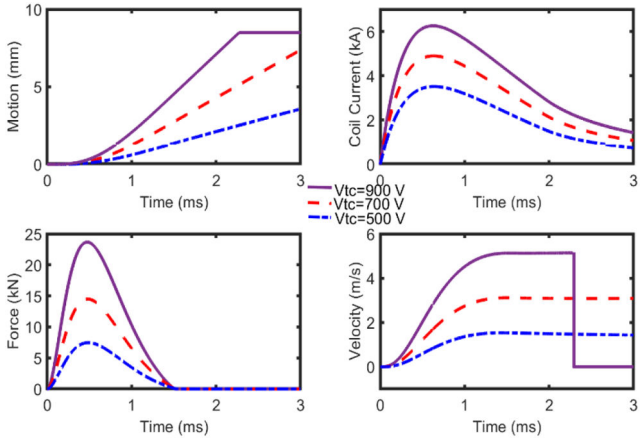

Fig. 11 *Speed, motion, coil current and the force of simulated 320 kV UFD*

μH/mm. Table 3 shows the final calculated electrical parameters. Table 4 presents the mechanical data of the 5 kV UFD.

To verify the 5 kV UFD electrodynamic model, the experiments have been conducted where the position of each contact is measured using the Hall effect sensor. The experiments are repeated for different charging voltages of TC capacitor, i.e. 300, 200 and 180 V. Fig. 10 presents the measured and simulated motion curves (z_g). As can be seen, the armature reaches its final position (3 mm) at about 1.5 ms in case of 300 V capacitor voltage. Some bounce is observed since no dampers are used, which is not included in the PSCAD model. With lower voltages, the stroke is incomplete because of high friction and bi-stable force. Good agreement between experiments and simulations is evident.

5.2 320 kV test UFD

The parameters of a 320 kV UFD have been estimated based on the work in [6, 18, 19], considering the reported opening time, contact velocity, dimensions of the armature and developed forces. Key design parameters are summarised in Table 4 while the calculated TC and TC driver parameters are given in Table 1. 33-mF capacitor banks with charging voltage of 900 V provides the required energy for two 20-turn TC to reciprocally move of the contacts and push/pull rod with the weight of about 3.5 kg. The peak voltage of 1.5 p.u. is considered resulting in the total gap distance of about 60 mm assuming one bar SF_6. Five breaking points are assumed, as shown in [19]. Considering 4.25 mm overlap, the maximum stroke travel is about 8.5 mm. Table 3 presents the calculated electrical parameters.

The performance of 320 kV UFD model is evaluated in the case of 900, 700 and 500 V voltage of the TC capacitor bank. Fig. 11 presents the results for the operation speed, motion, coil current, and the electromagnetic force. Theoretically, this UFD could operate within 2–3 ms for considered voltages, while the speed, TC coil current and the force would lie within the range of 1.5–6 m/s, 5–7 kA and 5–25 kN, respectively. The results are compatible with the ranges of these parameters reported in [6, 19]. Considering the reported opening time of 2 ms [4] the charging voltage of 900 V is adopted.

6 UFD failure mode validation and verification

6.1 Air insulated UFD

The validation of the air arc model from Section 4.2 has been performed on the downscale 5 kV UFD prototype. The arc model parameters are summarised in Table 5. Fig. 12 shows the experimental results with two test cases – opening at a current of 200 A (high) and opening at a current of 2.5 A (low). The arc voltages are calculated using (16), based on the current (Figs. 12*b* and *c*) and position sensor (Fig. 12*a*) measurements. These comparisons show a very good accuracy which validates the proposed air arc model.

Table 5 Electric arc parameters in air for a 5 kV UFD

Current, A	Gap distance, mm	A	B
< 100	1	36.32	−0.124
	5	71.39	−0.186
> 100	1	13.04	0.098
	5	14.13	0.211

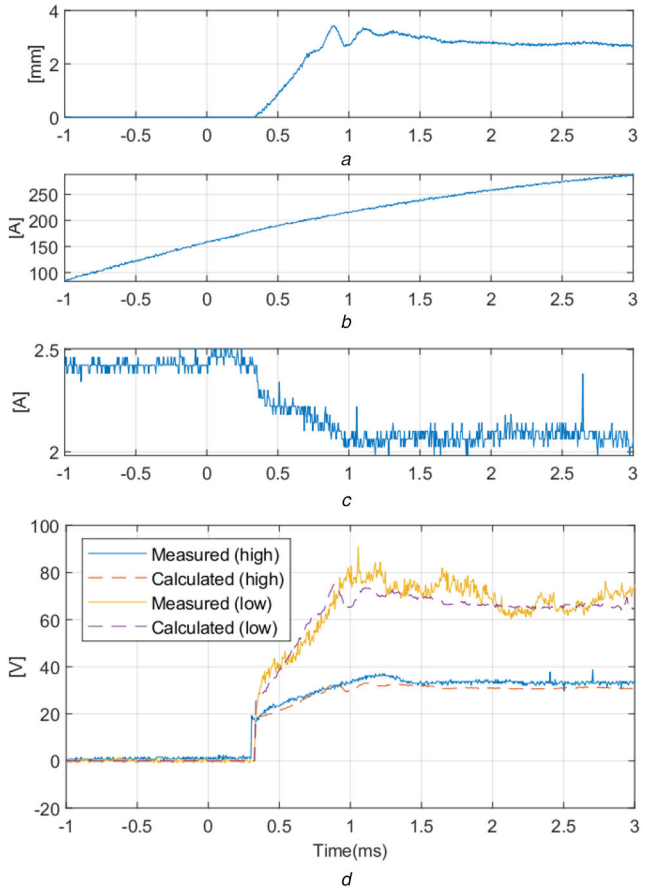

Fig. 12 *UFD air-arc model verification against measurements on 5 kV UFD*
(a) Gap distance, ***(b)*** Current (high), ***(c)*** Current (low), ***(d)*** Arc voltage

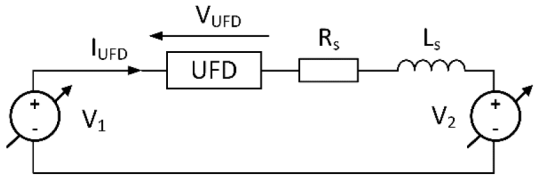

Fig. 13 *UFD test system model*

Table 6 Test parameters for a 320 kV UFD arc model

Parameter	Symbol	Test 1	Test 2
series inductance	L_s	0 mH	100 mH
series resistance	R_s	1 Ω	1 Ω
UFD chopping current	I_{chop}	1 A	1 A

6.2 SF_6 insulated UFD

The PSCAD test system for validating the SF_6 arc model based on (19) is shown in Fig. 13. It consists of two variable DC voltage sources V_1 and V_2 with series RL impedance. V_1 and V_2 represent two DC terminals in a VSC-based DC grid while the RL impedance represents a DC cable with a terminating inductor. In practice, the two DC voltages at cable ends can take a wide range of dynamically changing values, depending on the type of VSC converters, type of faults, and the protection system employed. Two tests are performed to demonstrate the applicability of the SF_6 arc model as shown in Table 6.

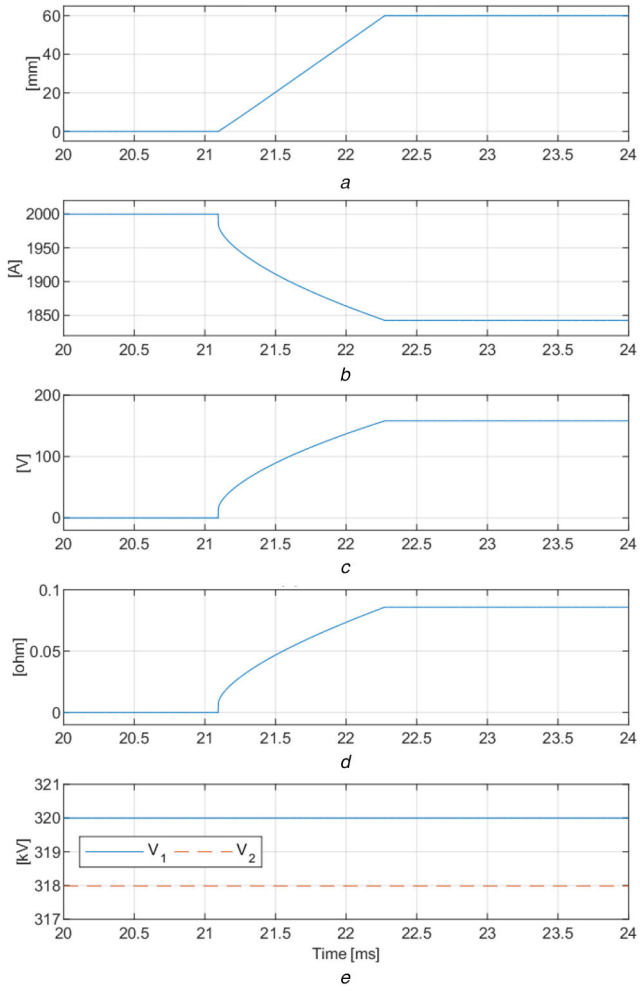

Fig. 14 *Attempted 320 kV UFD opening under load current*
(a) Total gap distance, ***(b)*** UFD current, ***(c)*** Arc voltage, ***(d)*** Arc resistance, ***(e)*** Source voltages

The results of the first test, simulating spurious opening under load current, are shown in Fig. 14. V_1 and V_2 are kept constant throughout the test while the series inductance is set to zero to speed up the current transient. The UFD opening command is given at 20 ms while the contact separation starts around 21.1 ms. The model enters arcing mode and the arc voltage increases with the gap distanced and reaches 158 V at full separation.

As the arc resistance increases, the current through the UFD decreases from 2 to 1.85 kA. Without corrective action from the control system (a change in source voltages), it is visible that the arcing in the UFD can cause a substantial change in the steady-state load current because the voltage difference between the terminals is typically low. However, in the actual HVDC system, this change may be slower because of the cable and DC CB inductances.

The second test, shown in Fig. 15, is developed to verify: (i) entering arc mode on high current; then (ii) exiting on low current; and (iii) entering failure mode on high voltage.

A DC fault condition with negative pre-fault current of −2 kA is assumed at 21 ms. At 21.1 ms, the UFD's contacts separate but, because $I_{UFD} > I_{chop}$, an arc is ignited between the contacts. The current is increasing at 3.2 kA/ms. At 21.63 ms, I_{UFD} falls below I_{chop} and the arc is temporarily extinguished, as seen by the spike in UFD voltage. However, at this point the contacts have not separated sufficiently to provide blocking voltage to satisfy $V_{UFD} > V_{max}$ and a restrike occurs due to dielectric breakdown. The arc is reignited and then the arc voltage continues to rise until full contact separation. Fig. 15*e* shows the net source voltage ($V_1 - V_2$),

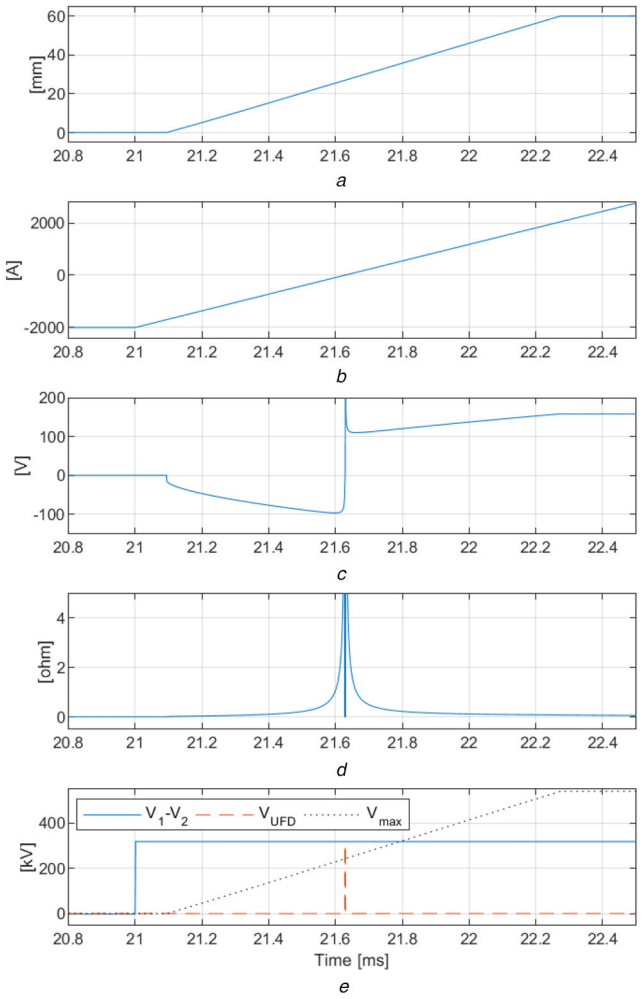

Fig. 15 *Simulation of SF_6 UFD model entering and exiting failure mode*
(a) Total gap distance, ***(b)*** UFD current, ***(c)*** Arc voltage, ***(d)*** Arc resistance, ***(e)*** Source and UFD voltages

as well as the UFD's actual voltage (V_{UFD}) and the maximum blocking voltage (V_{max}).

7 UFD inside DC CB

A UFD inside hybrid DC CB [4] will be located in the auxiliary branch, consisting of UFD and load commutation switch in series, which is in parallel with the main breaker branch. The presented UFD failure model is applicable for any external circuit given by voltage or current, including both states of the main branch: open or closed. The voltage across the main branch in the closed state will be several kV [7] which is an order of magnitude larger than the UFD arc voltage, as shown in Fig. 15. Therefore the fault current would still be directed through the UFD arc when the main branch is closed. The failure of hybrid DC CB and internal components is analysed in more detail in [17].

8 Conclusion

A system-level model for UFD is presented considering both normal operation and failure mode. It is concluded that Thomson coil inductances play a key role in the dynamics of the contacts movement and it is recommended to use finite element modelling for the particular design.

It is proposed to model the arcing of UFD using a variable resistance in series with an ideal switch. The variable resistance is calculated analytically based on the instantaneous position of contacts and the circuit electrical conditions. Two different arc models are recommended: for the air-insulated UFD and SF_6 UFD, and in each case, two operating regimes should be considered: high and low currents.

The UFD model is verified for both normal operation and failure mode using a 5 kV laboratory UFD and results show very good matching. The parameters for 320 kV SF_6 UFD model are presented and the model is evaluated using limited reported results from manufacturers.

9 Acknowledgments

This work was supported by the European Union's Horizon 2020 Research and Innovation Program under grant no. 691714. The authors thank Mr R. Osborne from the University of Aberdeen for help with the experimental studies.

10 References

[1] Jovcic, D: '*High voltage direct current transmission: converters systems and DC grids*' (Wiley, New Jersey, USA, **1**, 2nd edn 2019)
[2] Jovcic, D., Tang, G., Pang, H.: 'Adopting circuit breakers for high voltage dc networks: appropriating the vast advantages of dc transmission grids', *IEEE Power Energy Mag.*, 2019, **17**, (4), pp. 82–93
[3] CIGRE joined WG A3 and B4.34.: 'Technical requirements and specifications of state of the art HVDC switching equipment', CIGRE brochure 683, April 2017
[4] Häfner, J., Jacobson, B.: 'Proactive hybrid HVDC breakers – a key innovation for reliable HVDC grids'. Proc. CIGRE 2011 Bologna Symp., Bologna, Italy, September 2012, pp. 1–7
[5] Grieshaber, W., Dupraz, J., Penache, D., *et al.*: 'Development and test of a 120 kV direct current circuit breaker'. Proc. CIGRÉ Session, Paris, France, August 2014, pp. 1–11
[6] Skarby, P., Steiger, U.: 'An ultra-fast disconnecting switch for a hybrid HVDC breaker – a technical breakthrough'. Proc. CIGRÉ Session, Alberta, Canada, September 2013, pp. 1–9
[7] Hassanpoor, A., Häfner, J., Jacobson, B.: 'Technical assessment of load commutation switch in hybrid HVDC breaker', *IEEE Trans. Power Electron.*, 2015, **30**, (1), pp. 5393–5400
[8] Ruffing, P., Collath, N., Brantl, C., *et al.*: 'DC fault control and high-speed switch design for an HVDC network protection based on fault-blocking converters', *IEEE Trans. Power Deliv.*, 2019, **34**, (1), pp. 397–406
[9] Jovcic, D., Lin, W., Nguefeu, S., *et al.*: 'Low energy protection system for DC grids based on full bridge MMC converters', *IEEE Trans. Power Deliv.*, 2018, **33**, (4), pp. 1934–1943
[10] Jovcic, D., Zaja, M., Hedayati, M.: 'Bidirectional hybrid HVDC CB with a single HV valve', *IEEE Trans. Power Deliv.*, 2020, **35**, pp. 269–277, doi: 10.1109/TPWRD.2019.2912832
[11] Hedayati, M, Jovcic, D.: 'Reducing peak current and energy dissipation in hybrid HVDC CBs using disconnector voltage control', *IEEE Trans. Power Deliv.*, 2018, **33**, (4), pp. 2030–2038
[12] Jovcic, D.: 'Fast commutation of DC current into a capacitor using moving contacts', *IEEE Trans. Power Deliv.*, 2020, **35**, pp. 639–646, doi: 10.1109/TPWRD.2019.2919725
[13] Ritter, A., Franck, C. M.: 'Prediction of bus-transfer switching in future HVdc substations', *IEEE Trans. Power Deliv.*, 2018, **33**, (3), pp. 1388–1397
[14] Ritter, A., Straumann, U., Franck, C. M.: 'Novel method for predicting limit performance of bus-transfer switching by disconnectors', *IEEE Trans. Power Deliv.*, 2017, **32**, (5), pp. 2210–2217
[15] Ritter, A., Straumann, U., Franck, C. M.: 'Improving GIS disconnectors for future HVDC applications', *IEEE Trans. Power Deliv.*, 2018, **34**, (1), pp. 160–168
[16] Lin, W., Jovcic, D., Nguefeu, S., *et al.*: 'Modelling of high power hybrid DC circuit breaker for grid level studies', *IET Power Electron.*, 2016, **9**, (2), pp. 237–246
[17] Jovcic, D., Azizian Fard, M., Zaja, M.: 'Failure mode analysis of hybrid DC circuit breakers'. Cigre Int. Colloquium 2019, Johannesburg, South Africa, 1–4 October 2019, p. 12
[18] Bissal, A.: 'Modeling and Verification o Ultrafast Electromechnaical Actuators for HVDC Breakers', PhD Theiss, KTH, Stockholm, 2015
[19] ABB Schweiz AG.: 'Fast switch with Thomson coil and damping', European Patent Application EP 2 546 847 A1, 2013
[20] Olsson, H., Åström, K.J., De Wit, C.C., *et al.*: 'Friction models and friction compensation', *Eur. J. Control*, 1998, **4**, (3), pp. 176–195
[21] Li, X., Zou, J., Geng, L., *et al.*: 'Experiment research on current chopping on zero period of DC vacuum circuit breaker breaking'. 2017 4th Int. Conf. on Electric Power Equipment – Switching Technology (ICEPE-ST), Xi'an, 2017, pp. 389–392
[22] Paukert, J.: 'The arc voltage and arc resistance of LV fault arcs'. Proc.7th Int. Symp. Switching Arc Phenom., Lodz, Poland, 1993, pp. 49–51
[23] Ammerman, R. F., Gammon, T., Sen, P. K., *et al.*: 'DC-Arc Models and incident-energy calculations', *IEEE Trans. Ind. Appl.*, 2010, **46**, (5), pp. 1810–1819
[24] Koch, D.: 'SF_6 properties and use in MV and HV switchgear', Schneider Electric, Grenoble, France, 2003
[25] Yokomizu, Y., Matsumura, T., Henmi, R., *et al.*: 'Total voltage drops in electrode fall regions of SF_6, argon and air arcs in current range from 10 to 20 000 A', *J. Phys. D, Appl. Phys.*, 1996, **29**, (5), pp. 1260–1267
[26] Wheeler, H.A.: 'Simple inductance formulas for radio coils', *Proc. of the Institute of Radio Eng.*, 1928, **16**, (10), pp. 1398–14000